Received: 3 March 2021 | Revised: 5 May 2021 | Accepted: 17 June 2021

DOI: 10.1111/cas.15046

ORIGINAL ARTICLE

Cancer Science WILEY

Ca^{2+}-activated K^+ channel $K_{Ca}1.1$ as a therapeutic target to overcome chemoresistance in three-dimensional sarcoma spheroid models

Susumu Ohya[1] | Junko Kajikuri[1] | Kyoko Endo[1] | Hiroaki Kito[1] | Elghareeb E. Elboray[2,3] | Takayoshi Suzuki[2]

[1]Department of Pharmacology, Graduate School of Medical Sciences, Nagoya City University, Nagoya, Japan

[2]Department of Complex Molecular Chemistry, The Institute of Scientific and Industrial Research, Osaka University, Osaka, Japan

[3]Faculty of Science, South Valley University, Qena, Egypt

Correspondence
Susumu Ohya, Department of Pharmacology, Graduate School of Medical Sciences, Nagoya City University, Nagoya, Japan.
Email: sohya@med.nagoya-cu.ac.jp

Funding information
A JSPS KAKENHI Grant, Grant/Award Number: JP20K07071

Abstract

The large-conductance Ca^{2+}-activated K^+ channel $K_{Ca}1.1$ plays a pivotal role in tumor development and progression in several solid cancers. The three-dimensional (3D) in vitro cell culture system is a powerful tool for cancer spheroid formation, and mimics in vivo solid tumor resistance to chemotherapy in the tumor microenvironment (TME). $K_{Ca}1.1$ is functionally expressed in osteosarcoma and chondrosarcoma cell lines. $K_{Ca}1.1$ activator-induced hyperpolarizing responses were significantly larger in human osteosarcoma MG-63 cells isolated from 3D spheroid models compared with in those from adherent 2D monolayer cells. The present study investigated the mechanisms underlying the upregulation of $K_{Ca}1.1$ and its role in chemoresistance using a 3D spheroid model. $K_{Ca}1.1$ protein expression levels were significantly elevated in the lipid-raft-enriched compartments of MG-63 spheroids without changes in its transcriptional level. 3D spheroid formation downregulated the expression of the ubiquitin E3 ligase FBXW7, which is an essential contributor to $K_{Ca}1.1$ protein degradation in breast cancer. The siRNA-mediated inhibition of FBXW7 in MG-63 cells from 2D monolayers upregulated $K_{Ca}1.1$ protein expression. Furthermore, a treatment with a potent and selective $K_{Ca}1.1$ inhibitor overcame the chemoresistance of the MG-63 and human chondrosarcoma SW-1353 spheroid models to paclitaxel, doxorubicin, and cisplatin. Among several multidrug resistance ATP-binding cassette transporters, the expression of the multidrug resistance-associated protein MRP1 was upregulated in both spheroids and restored by the inhibition of $K_{Ca}1.1$. Therefore, the pharmacological inhibition of $K_{Ca}1.1$ may be an attractive new strategy for acquiring resistance to chemotherapeutic drugs in the TME of $K_{Ca}1.1$-positive sarcomas.

Abbreviations: 2D/3D, two/three-dimension(al); ABC, ATP-binding cassette; ACTB, β-actin; CIS, cisplatin; CN, calcineurin; CRBN, cereblon; CS, chondrosarcoma; $DiBAC_4(3)$, bis-(1,3-dibutylbarbituric acid)trimethine oxonol; DOX, doxorubicin; ERK, extracellular signal-regulated kinase; FBXW, F-box and WD repeat domain-containing; Fura 2-AM, acetoxymethyl 2-[5-[bis[(acetoxymethoxy-oxo-methyl)methyl]amino]-4-[2-[2-[bis[(acetoxymethoxy-oxo-methyl)methyl]amino]-5-methyl-phenoxy]ethoxy]benzofuran-2-yl]oxazole-5-carboxylate; HDAC, histone deacetylase; HIF, hypoxia-inducible factor; IL, interleukin; K_{Ca}, Ca^{2+}-activated K^+ (channel); LRRC, leucine-rich repeat-containing protein; MAPK, mitogen-activated protein kinase; MDM, murine double minute; MDR, multidrug resistance; MRP, multidrug resistance-associated protein; mTOR, mechanistic target of rapamycin; NAD, nicotinamide adenine dinucleotide; NFAT, nuclear factor of activated T cell; NRF, nuclear factor erythroid 2-related factor; OS, osteosarcoma; PAC, paclitaxel; PAX, paxilline; PI3K, phosphoinositide 3-kinase; RIPA, radioimmunoprecipitation assay; SIRT, sirtuin; TME, tumor microenvironment.

KEYWORDS
Ca^{2+}-activated K^+ channel $K_{Ca}1.1$, cancer spheroid model, chemoresistance, FBXW7, MRP1, sarcoma

1 | INTRODUCTION

Potassium (K^+) channels play a critical role in the proliferation, apoptosis, migration, adhesion, and metastasis of cancer cells by controlling cell volumes and Ca^{2+} signaling.[1] The large-conductance Ca^{2+}-activated K^+ channel $K_{Ca}1.1$ (also known as BK, BK_{Ca}, Maxi-K, and Slo1) encoded by the *KCNMA1* gene has been implicated in tumor development and progression in breast, prostate, cervical, renal, and colorectal cancers and glioma, by promoting the driving force of Ca^{2+} influx through voltage-independent Ca^{2+} channels.[1,2] The amplification of *KCNMA1* correlated with a high tumor stage and poor prognosis in breast cancer,[3] and has potential as a tumor grade-associated marker of prostate cancer.[4] The functional diversity of $K_{Ca}1.1$ is due to the alternative splicing of the $K_{Ca}1.1$ α subunit and its kinetic modulation by the auxiliary β (β1-4) and γ (γ1-4) subunits.[5,6] $K_{Ca}1.1$ is distributed in "lipid rafts," which are cholesterol-enriched nanodomains, in cancer cells and contributes to the fine-tuning of cancer-associated functions, such as proliferation, migration, and metastasis.[7]

Bone sarcoma accounts for more than 10% of all sarcomas. Osteosarcoma (OS) is the most common malignant bone tumor in children and adolescents.[8] Chemotherapy is an important strategy for the treatment of patients with high-grade OS.[9] Chondrosarcoma (CS) is the second most common primary malignancy of bone and is resistant to both chemotherapy and radiation.[10] There are currently no promising drugs available for CS. $K_{Ca}1.1$ is functionally expressed in human OS and CS cell lines[11,12]; however, limited information is currently available in its therapeutic significance in the tumor microenvironment (TME).

The hypoxic TME promotes cancer progression and survival.[13,14] The overexpression of hypoxia-inducible factor (HIF)-1α has been shown to correlate with a poor patient prognosis, and promotes the resistance of solid tumors to chemo- and radiotherapies.[13-15] HIF-1α also promotes cancer stemness. Three-dimensional (3D) in vitro cancer spheroid models mimic the TME of human solid tumors, and are an efficient tool for investigating metastasis, invasion, chemoresistance and radioresistance, and stemness.[16,17] Histone deacetylases (HDACs) are classified into 4 groups: classes I, II, III, and IV, and HDAC3 and sirtuin 1 (SIRT1), belonging to classes I and III, respectively, regulate hypoxia-induced metastasis and chemoresistance in a wide range of cancer types.[18,19] NAD-dependent SIRT1 is downregulated by decreased NAD^+ levels under hypoxic TME.[20] Furthermore, low SIRT1 levels predict poor survival and metastasis in breast cancer.[21,22]

Recent studies have implicated ion channels in chemoresistance to cisplatin (CIS), doxorubicin (DOX), and paclitaxel (PAC).[23] ABC transporters play a major role in the acquisition of chemoresistance, to which the multidrug resistance-associated protein MRP1 is a key contributor. MRP1 is upregulated through the nuclear factor erythroid 2-related factor 2, NRF2 signaling pathways, that play an essential role in poor prognosis and chemoresistance in cancer.[24-26]

A recent study has reported that antiandrogen-induced $K_{Ca}1.1$ protein degradation was mediated by the ubiquitin E3 ligases, F-box and WD repeat domain-containing (FBXW7), and murine double minute (MDM2) in a $K_{Ca}1.1$-expressing breast cancer cell line.[27] FBXW7 is a tumor suppressor gene and its downregulation has been shown to promote tumor stemness by preventing the protein degradation of stemness regulators, such as c-*Myc* and Sox2.[28] A previous study has demonstrated that the loss of FBXW7 increased chemoresistance, and showed that cancer spheroid formation-mediated chemoresistance was positively associated with the hypoexpression of FBXW7.[29]

The objective of the present study was to elucidate the mechanisms underlying the post-translational modification of $K_{Ca}1.1$ and the therapeutic significance of its functions in the TME using a 3D spheroid culture system in $K_{Ca}1.1$-expressing sarcoma cells.

2 | MATERIALS AND METHODS

2.1 | Chemicals

Paxilline (PAX; Cayman Chemical), NS1619 (Abcam), DOX hydrochloride (FUJIFILM Wako Pure Chemical), PAC (FUJIFILM Wako Pure Chemical), CIS (FUJIFILM Wako Pure Chemical), $DiBAC_4(3)$ (DOJINDO), Fura-2 AM (DOJINDO), and siRNA for FBXW7 (Thermo Fisher Scientific) were purchased. HDAC/SIRT inhibitors (vorinostat and NCO-01) were provided by Prof. Takayoshi Suzuki (Osaka Univ., Osaka, Japan). The other chemicals used in the present study were from Sigma-Aldrich, FUJIFILM Wako Pure Chemical, and Nacalai Tesque unless otherwise stated.

2.2 | Cell culture

The human OS cell line MG-63 and CS cell line SW-1353 were purchased from the RIKEN Cell Bank. The lines were cultured in D-MEM medium (FUJIFILM Wako Pure Chemical) supplemented with 10% fetal bovine serum (Sigma-Aldrich Japan) and penicillin (100 units/mL)/streptomycin (100 μg/mL) mixture (FUJIFILM Wako Pure Chemical). All cells were cultured in a humidified atmosphere containing 5% CO_2 in air at 37°C. Flat-bottomed dishes and plates (Corning) were used in the two-dimensional (2D) cell culture. The PrimeSurface® system (Sumitomo Bakelite) was used for 3D spheroid formation. Cell suspensions of MG-63 and SW-1353 were

seeded onto a PrimeSurface 96 U plate at 10^4 cells/well and then cultured for 3-4 d.

2.3 | RNA extraction, cDNA synthesis, and real-time PCR

Total RNA was isolated from cancer cells by the conventional acid guanidium thiocyanate-phenol-chloroform method. The concentration and quality of RNA were confirmed using a microvolume spectrophotometer, NanoDrop One (Thermo Fisher Scientific). Reverse transcription was performed using ReverTra Ace (ToYoBo) with random hexanucleotides. Quantitative real-time PCR was performed using the Luna Universal qPCR Master Mix (New England Biolabs Japan) and the Applied Biosystems 7500 Fast Real-Time PCR system (Thermo Fisher Scientific). PCR primers of human origin are listed in Table S1. The relative expression levels were calculated using the $2^{-\Delta\Delta Ct}$ method and normalized to β-actin (ACTB).[27]

2.4 | Western blots

Lipid raft-enriched protein fraction lysates were extracted using the ULTRARIPA kit for Lipid Rafts (BioDynamics Laboratory) in accordance with the manufacturer's instructions. Whole cell lysates were extracted using RIPA buffer. Equal amounts of protein were subjected to SDS-PAGE and immunoblotting with anti-$K_{Ca}1.1$ polyclonal (rabbit; approximately 100 kDa; APC-021, Alomone Labs), anti-FBXW7 polyclonal (rabbit; app. 70 kDa; A5872, ABclonal), anti-SIRT1 polyclonal (rabbit; app. 130 kDa; Medical & Biological Laboratories, MBL), anti-HDAC3 polyclonal (rabbit; app. 50 kDa; H-99, SCB), anti-MRP1 polyclonal (rabbit; app. 250 kDa; bs-0657R, Bioss Antibodies), and anti-ACTB monoclonal (mouse; 43 kDa; 6D1, MBL) antibodies, and were then incubated with anti-rabbit or anti-mouse horseradish peroxidase-conjugated IgG (Merck Millipore). An enhanced chemiluminescence detection system (GE Healthcare Japan) was used to detect the bound antibody. The resulting images were analyzed using an Amersham Imager 600 (GE Healthcare Japan). The optical density of the protein band signal relative to that of the ACTB signal was calculated using ImageJ software (v.1.42, NIH), and protein expression levels in the vehicle control were then expressed as 1.0.

2.5 | Measurement of the membrane potential and intracellular Ca^{2+} concentrations by fluorescence indicators

The membrane potential was measured using the fluorescence voltage-sensitive dye $DiBAC_4(3)$, as previously reported.[27] The cells were continuously incubated with 100 nmol/L $DiBAC_4(3)$ throughout the experiments. In membrane potential imaging, cells loaded with $DiBAC_4(3)$ were illuminated at a wavelength of 490 nm. The intracellular Ca^{2+} concentrations were measured using the fluorescent Ca^{2+} indicator dye Fura 2-AM (DOJINDO). Cells were incubated with 10 μmol/L Fura 2-AM for 30 min at room temperature. Cells loaded with Fura 2 were alternatively illuminated at wavelengths of 340 and 380 nm. Fluorescence images were recorded on an ORCA-Flash2.8 digital camera (Hamamatsu Photonics). Data collection and analyses were performed using an HCImage system (Hamamatsu Photonics). Images were measured every 5 s, and the values of fluorescence intensity (F) were determined by measuring the average for 1 min (12 images). The fluorescence intensity of Fura 2 was expressed as measured 340/380 nm fluorescence ratios after background subtraction.

2.6 | Cell viability assay

A cell viability assay was performed in accordance with our previous study.[27] Briefly, using a density of 10^4 cells/mL, cells were cultured in duplicate in 96-well plates for 4-5 d (for the 3D culture) and 1 d (for the 2D culture). Cells were then treated with the drugs used for chemotherapy (PAC, DOX, and CIS) for 2 d. At 2 h after the addition of WST-1 reagent (DOJINDO) to each well, absorbance was measured using a microplate reader SpectraMax 384 (Molecular Devices Japan) at a test wavelength of 450 nm and reference wavelength of 650 nm.

2.7 | Cell cycle distribution

In the cell cycle distribution analysis, isolated cells were fixed overnight in ice-cold 70% ethanol. Fixed cells were stained with PBS containing propidium iodide (10 μg/mL) and DNase-free RNase (0.1 mg/mL). Stained cells were subjected to a flow cytometric analysis (FACSCanto II, BD Biosciences) acquiring at least 10 000 events. Data were analyzed using BD FACSDiva software.

2.8 | Immunocytochemistry assay for cell imaging

Fixed and non-permeabilized cells were stained with an anti-$K_{Ca}1.1$ polyclonal antibody (rabbit; extracellular, APC-151, Alomone Labs) followed by an Alexa Fluor 488-conjugated secondary antibody (Thermo Fisher Scientific), and then analyzed by flow cytometry (FACSCanto II, BD Biosciences).

2.9 | Statistical analysis

Statistical analyses were performed using Statistical software XLSTAT (version 2013.1). To assess the significance of differences between the 2 groups and among multiple groups, unpaired/paired Student *t* tests with Welch correction or Tukey tests were used. Results with a *P*-value of less than .05 were considered to be significant. Data were presented as means ± SEM.

3 | RESULTS

3.1 | $K_{Ca}1.1$ activity in isolated cells from MG-63 and SW-1353 spheroids

Previous studies have reported that the OS and CS cell lines, MG-63 and SW-1353, functionally express $K_{Ca}1.1$.[11,12] 3D spheroid model generation from these cell lines was performed using the ultra-low attachment cultureware, PrimeSurface 96 U. At 4 d after cell seeding, spheroidal aggregates of cancer cells were formed in both cell lines (Figures 1A and 2A). Hyperpolarizing responses induced by the $K_{Ca}1.1$ activator, NS1619, were significantly larger in acutely isolated MG-63 cells from 3D spheroids (n = 19) than in those from 2D adherent cell monolayers (n = 18; $P < .01$; Figure 1B,C). Pretreatment with the selective $K_{Ca}1.1$ blocker, PAX (5 μmol/L) significantly reduced NS1619-induced hyperpolarizing responses (approximately 80%, n = 11). We then examined the gene and protein expression levels of $K_{Ca}1.1$ in MG-63 cells using real-time PCR and western blot assays. The expression level of the $K_{Ca}1.1$ protein with a molecular weight of approximately 100 kDa was increased in MG-63 spheroids (n = 4 for each, $P < .01$; Figure 1D,E), without changes in that of the $K_{Ca}1.1$ transcript (Figure 1G). Consistent with our previous findings,[27] the band signal specific for $K_{Ca}1.1$ almost completely disappeared following the pretreatment with the primary antibody with excess antigen (not shown). The results of the flow cytometric analysis using the Alexa Fluor 488-conjugated antibody against the extracellular domain of human $K_{Ca}1.1$ indicated a significantly higher mean fluorescence intensity in MG-63 cells

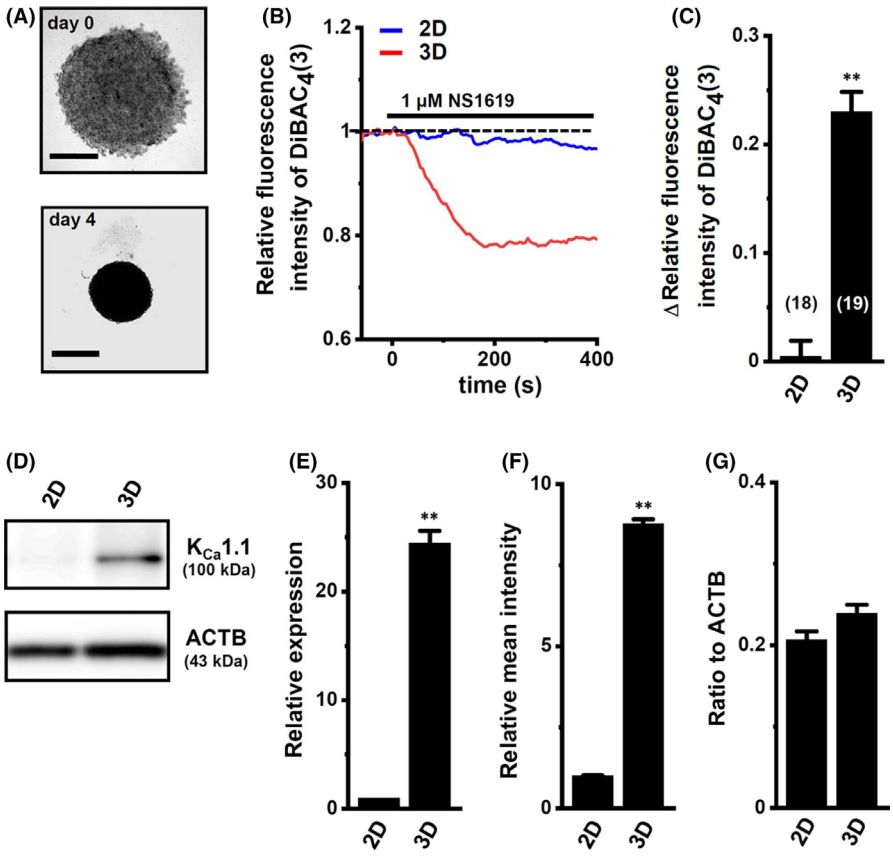

FIGURE 1 Comparison of Ca^{2+}-activated K^+ channel $K_{Ca}1.1$ expression and activity between human OS MG-63 cells cultured as 2D monolayers and 3D spheroids. A, Phenotypic properties of MG-63 cells cultured with ultra-low attachment PrimeSurface 96 U plates (upper panel: day 0, lower panel: day 4). Brightfield images were obtained with the Axio Observer Z1 microscope system (Carl Zeiss). Bars show 50 μm. B, Time course of the voltage-sensitive fluorescent dye imaging of $K_{Ca}1.1$ activator (1 μmol/L NS1619)-induced hyperpolarizing responses in isolated cells from 2D monolayers ("2D") and 3D spheroids ("3D") of MG-63. The fluorescence intensity of $DiBAC_4(3)$ before the application of NS1619 is expressed as 1.0. Images were measured every 5 s. C, Summarized results of NS1619-induced hyperpolarizing responses in cells isolated from at least 3 different batches in each group. Cell numbers used in experiments are shown in parentheses. The values for fluorescence intensity were obtained by measuring the average for 1 min (12 images). D, $K_{Ca}1.1$ protein expression in the lipid raft-enriched protein lysates of both groups. Blots were probed with anti-$K_{Ca}1.1$ (approximately 100 kDa, upper panel) and anti-ACTB (43 kDa, lower panel) antibodies. E, Summarized results were obtained as the optical density of $K_{Ca}1.1$ and ACTB band signals. After compensation for the optical density of the $K_{Ca}1.1$ protein band signal with that of the ACTB signal, the $K_{Ca}1.1$ signal in "2D" was expressed as 1.0 (n = 4 for each). F, Fixed, non-permeabilized MG-63 cells were stained with an Alexa 488-fused anti-$K_{Ca}1.1$ (extracellular) antibody, and mean fluorescence intensities were measured using flow cytometry. Their values in "2D" were expressed as 1.0 (n = 4 for each). G, Real-time PCR examination of the $K_{Ca}1.1$ transcript in both groups (n = 4 for each). Expression levels were shown as a ratio compared with ACTB. Results are expressed as means ± SEM. $^{**}P < .01$ vs 2D

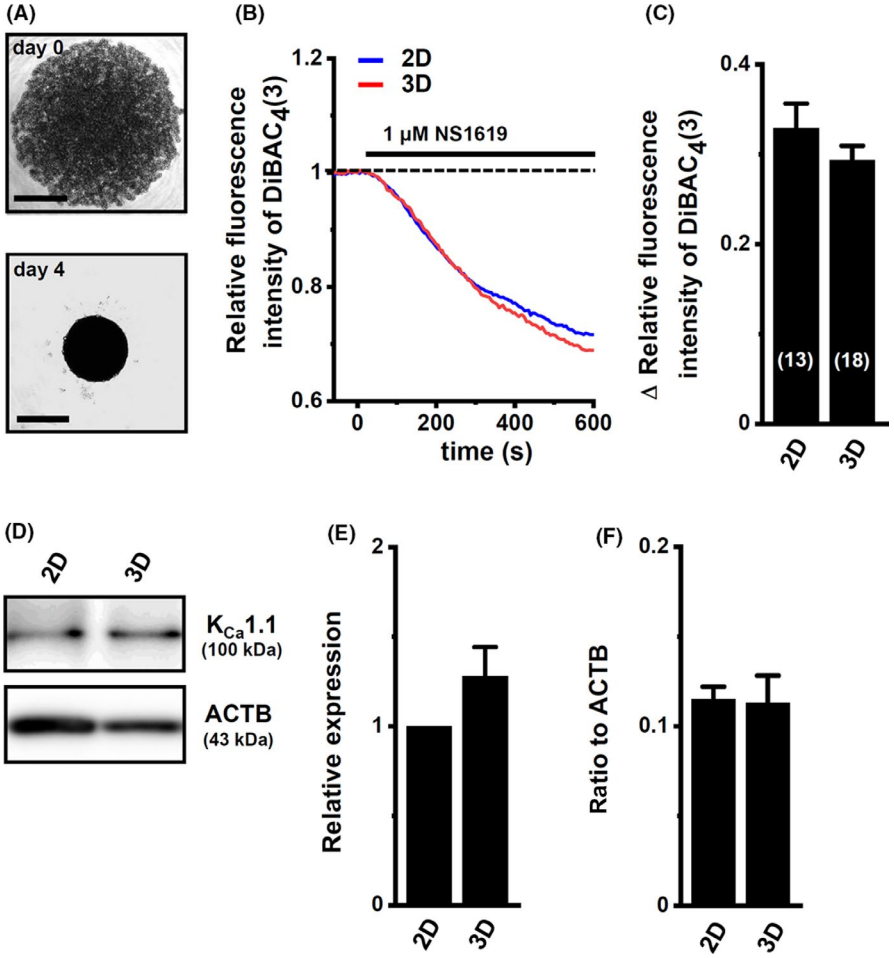

FIGURE 2 Comparison of $K_{Ca}1.1$ expression and activity between human CS SW-1353 cells cultured as 2D monolayers and 3D spheroids. A, Phenotypic properties of SW-1353 cells cultured with ultra-low attachment PrimeSurface 96 U plates (upper panel: day 0, lower panel: day 4). Bars show 50 μm. B, Time course of the voltage-sensitive fluorescent dye imaging of NS1619-induced hyperpolarizing responses in isolated cells from the 2D monolayers ("2D") and 3D spheroids ("3D") of SW-1353. The fluorescence intensity of $DiBAC_4(3)$ before the application of NS1619 was expressed as 1.0. Images were measured every 5 s. C, Summarized results of NS1619-induced hyperpolarizing responses in cells isolated from at least 3 different batches in each group. Cell numbers used in experiments are shown in parentheses. The values for fluorescence intensity were obtained by measuring the average for 1 min (12 images). D, $K_{Ca}1.1$ protein expression in the lipid raft-enriched protein lysates of both groups. Blots were probed with anti-$K_{Ca}1.1$ (approximately 100 kDa, upper panel) and anti-ACTB (43 kDa, lower panel) antibodies. E, Summarized results were obtained as the optical density of $K_{Ca}1.1$ and ACTB band signals. After compensation for the optical density of the $K_{Ca}1.1$ protein band signal with that of the ACTB signal, the $K_{Ca}1.1$ signal in "2D" was expressed as 1.0 (n = 4 for each). F, Real-time PCR examination of the $K_{Ca}1.1$ transcript in both groups (n = 4 for each). Expression levels were shown as a ratio to ACTB. Results are expressed as means ± SEM

from 3D spheroids than in those from 2D monolayers (Figure 1F). Conversely, NS1619-induced hyperpolarizing responses were observed in acutely isolated SW-1353 spheroids (n = 18); however, similar responses were also found in those from 2D monolayers (n = 13; $P > .05$; Figure 2B,C). Corresponding to these results, no significant differences were observed in the expression levels of $K_{Ca}1.1$ transcripts and proteins between 2D- and 3D-cultured SW-1353 cells (n = 4 for each, $P > .05$; Figure 2C-E). These results indicated that (a) $K_{Ca}1.1$ activity was high in both spheroids and (b) the decrease in $K_{Ca}1.1$ protein degradation or increase in the localization of the plasma membrane lipid rafts of $K_{Ca}1.1$ may be involved in enhancing $K_{Ca}1.1$ activity in MG-63 spheroids. The transcriptional expression levels of other K_{Ca} channels ($K_{Ca}2.x$ and $K_{Ca}3.1$) and the auxiliary β and γ subunits of $K_{Ca}1.1$, which affect channel kinetic properties, were very low (Figures S1 and S2).

3.2 | Downregulation of the ubiquitin E3 ligase, FBXW7 in MG-63 spheroids

To identify candidates involved in the protein degradation of $K_{Ca}1.1$ in MG-63 cells (see Section 1), we compared the expression levels of FBXW7, MDM2, and cereblon (CRBN) between the 2D monolayers and 3D spheroids of both sarcomas.[27,30] As shown in Figure 3A-C, the expression levels of FBXW7 transcripts and proteins were significantly decreased by spheroid formation in MG-63 cells.

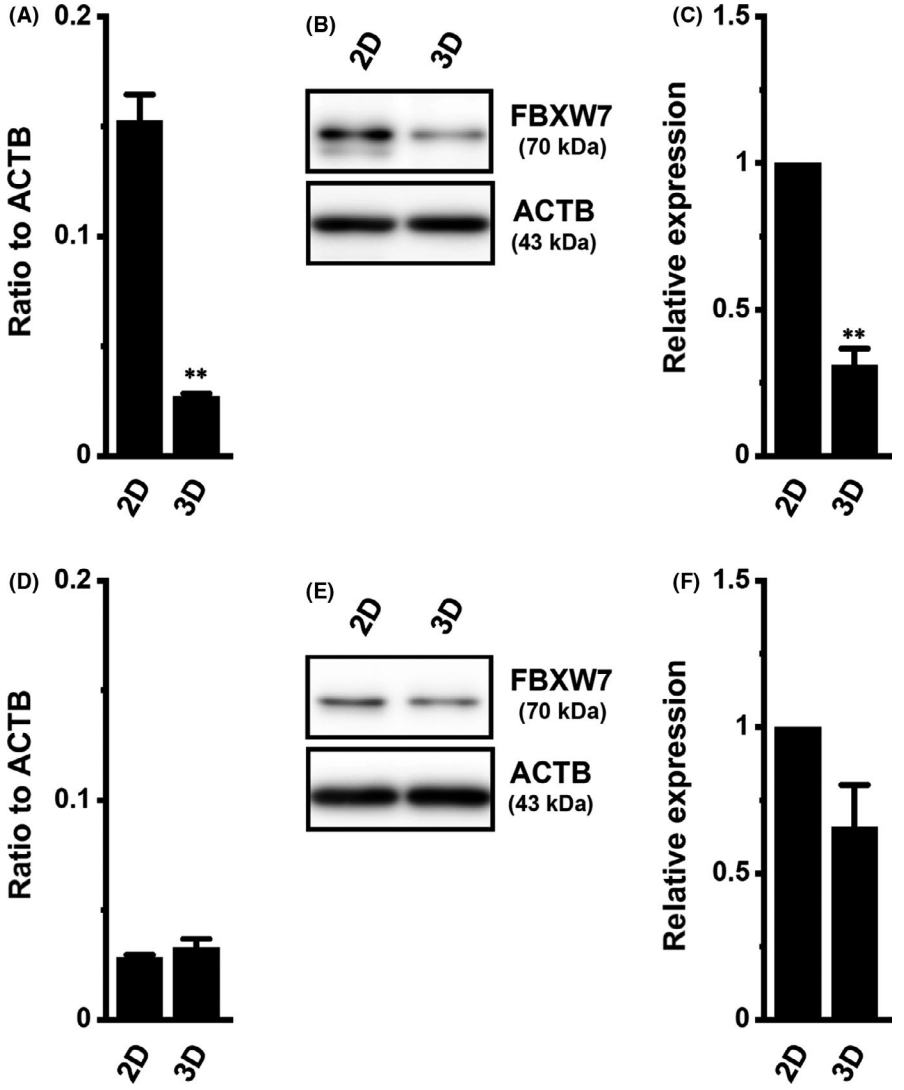

FIGURE 3 Comparison of expression levels of the ubiquitin E3 ligase, FBXW7 between 2D- and 3D-cultured sarcoma cells. Real-time PCR examination of FBXW7 transcripts in 2D monolayers ("2D") and 3D spheroids ("3D") of MG-63 (A) and SW-1353 (D) cells (n = 4 for each). Expression levels were shown as a ratio to ACTB. Protein expression of FBXW7 in protein lysates of both sarcomas. Blots were probed with anti-FBXW7 (approximately 70 kDa) and anti-ACTB (43 kDa) antibodies (B, E). Summarized results were obtained as the optical density of FBXW7 (C, F) band signals. After compensation for the optical density of the FBXW7 protein band signal with that of the ACTB signal, the optical density in "2D" was expressed as 1.0 (n = 4 for each). Results are expressed as means ± SEM. $^{**}P < .01$ vs 2D

Conversely, the expression levels of FBXW7 were significantly lower in the 2D monolayers of SW-1353 cells, and no significant changes in the expression levels of FBXW7 were noted in SW-1353 spheroids (Figure 3D-F). In both spheroids, a significant increase in the expression levels of MDM2 and CRBN (Figure S3) was observed, suggesting a negligible contribution to the regulation of $K_{Ca}1.1$ activity in both spheroids. The siRNA-mediated suppression of FBXW7 (Figure 4A) induced an increase in the expression level of the $K_{Ca}1.1$ protein by preventing FBXW7-mediated $K_{Ca}1.1$ protein degradation ($P < .01$; Figure 4B,C). These results strongly suggest that the decrease in FBXW7 expression is associated with the increase in $K_{Ca}1.1$ activity in MG-63 spheroids.

3.3 | Overcoming chemoresistance by $K_{Ca}1.1$ inhibition in both sarcoma spheroids

Cancer spheroid formation mimicking the TME promotes resistance to chemotherapy drugs, which is referred to as "chemoresistance."[16,17] PAC, DOX, and CIS are the most widely used chemotherapy drugs. As shown in Figures 5, 3D spheroids of MG-63 and SW-1353 cells exhibited chemoresistance to PAC, DOX, and CIS (n = 5 for each, $P < .01$). To investigate whether $K_{Ca}1.1$ is involved in the acquisition of chemoresistance, both sarcoma spheroids were pre-incubated with the selective $K_{Ca}1.1$ inhibitor PAX (10 μmol/L) for 24 h. As shown in Figure 6, sensitivity to chemotherapy drugs was significantly, but not completely, recovered by the PAX treatment (n = 5 for each, $P < .01$).

ABC transporters are responsible for drug resistance.[31] Therefore, we initially examined the expression levels of MDR1 (ABCB1), MRP1 (ABCC1), MRP2 (ABCC2), and BCRP1 (ABCG2), possible target molecules transporting chemotherapy drugs, using real-time PCR. The expression levels of MRP1 transcripts were significantly higher in the 3D spheroids of both cells than in 2D monolayers (n = 4 for each, $P < .01$; Figure 7A,D). The other ABC transporters were rarely expressed in any group, with expression levels of less than 0.002 in arbitrary units. Corresponding to the results obtained on transcriptional expression, the expression levels of MRP1 proteins were significantly increased in the 3D spheroids of both cells (n = 4 for each, $P < .01$ and .05 vs 2D in MG-63 and SW-1353, respectively; Figure 7B,C,E,F).

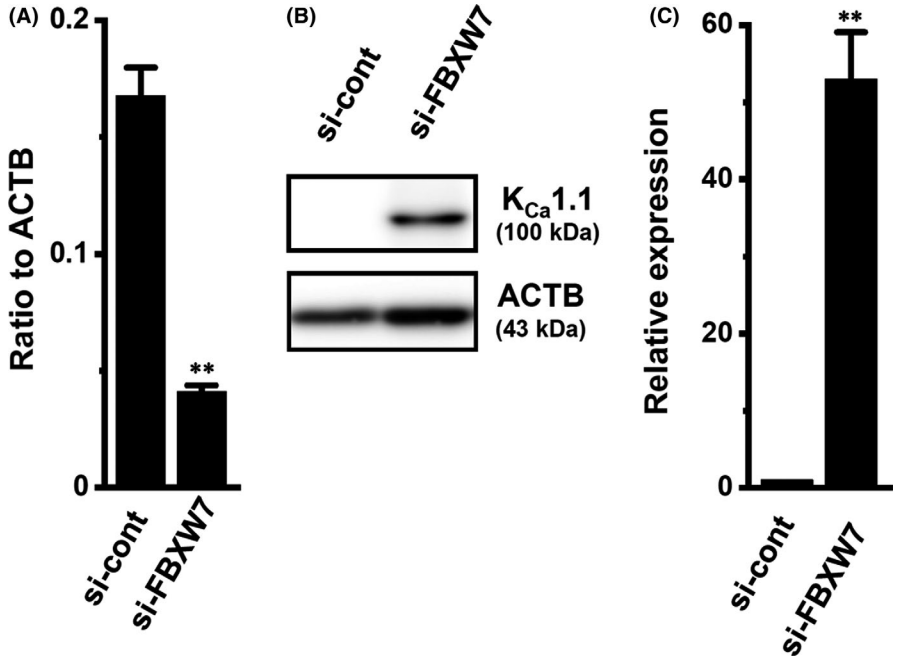

FIGURE 4 Effects of the siRNA-mediated inhibition of FBXW7 on expression levels of the K_{Ca}1.1 protein in 2D-cultured MG-63 cells. A, Real-time PCR examination of FBXW7 transcripts in control siRNA (si-cont)- and FBXW7 siRNA (si-FBXW7)-transfected 2D monolayers of MG-63 cells (n = 4 for each). Expression levels are shown as a ratio compared with ACTB. Protein expression of K_{Ca}1.1 in si-cont and si-FBXW7 groups. Blots were probed with anti-K_{Ca}1.1 (approximately 100 kDa) and anti-ACTB (43 kDa) antibodies (B). Summarized results were obtained as the optical density of K_{Ca}1.1 band signals (C). After compensation for the optical density of the K_{Ca}1.1 protein band signal with that of the ACTB signal, the optical density in "si-cont" was expressed as 1.0 (n = 4 for each). Results are expressed as means ± SEM. $^{**}P < .01$ vs si-cont

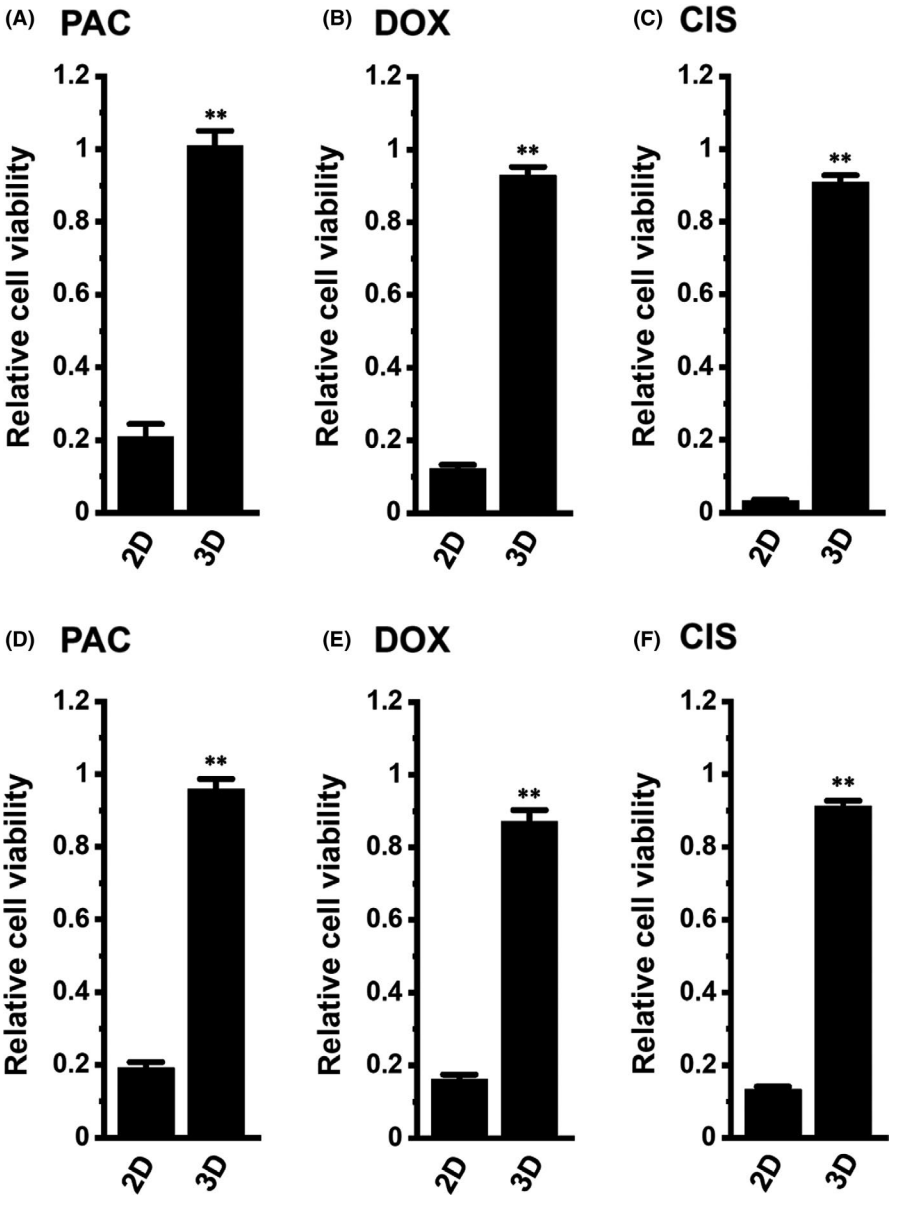

FIGURE 5 Effects of chemotherapeutic reagents on the viability of 2D- and 3D-cultured MG-63 and SW-1353 cells. Effects of the treatment with 100 nmol/L paclitaxel (PAC), 1 μmol/L doxorubicin (DOX), and 10 μmol/L cisplatin (CIS) for 48 h on the viability of 2D- and 3D-cultured MG-63 (A-C) and SW-1353 (D-F) cells using the WST-1 assay. Cell viability in "2D" was expressed as 1.0. Results are expressed as means ± SEM. $^{**}P < .01$ vs 2D

Consistent with the $K_{Ca}1.1$ inhibition overcoming chemoresistance (Figure 6), the expression levels of MRP1 transcripts and proteins were recovered by treatment with PAX for 24 h in both spheroids (n = 4 for each, $P < .01$; Figure 8). No changes were observed in the transcriptional expression levels of the other ABC transporters following the PAX treatment in both spheroids (less than 0.002 in arbitrary units).

3.4 | HDAC-mediated epigenetic regulation of FBXW7 in sarcoma spheroids

In the present study, the mechanisms underlying the downregulation of FBXW7 in spheroid formation have not yet been elucidated (Figure 3). FBXW7 is epigenetically modified in cancer cells.[32,33] Furthermore, previous studies have reported that, among the 18 members of class I-IV HDACs, HDAC3, SIRT1, and SIRT2, belonging to classes I and III, were regulated in the TME of a wide range of cancer types.[18,19] As shown in Figure 9, the expression levels of HDAC3 and SIRT1 transcripts and proteins were significantly decreased in MG-63 spheroids (n = 4 for each, $P < .01$). The expression levels of SIRT2 transcripts were significantly lower compared with those of HDAC3 and SIRT1 transcripts, and no significant differences were noted between 2D and 3D (Figure 9C). To clarify the involvement of HDAC3 and/or SIRT1 in the expression of FBXW7 in MG-63 cells, we examined the effects of treatments with the HDAC inhibitors vorinostat (10 μmol/L for class I, II, and IV HDAC subtypes) and NCO-01 (50 μmol/L for class III SIRT1/2) for 24 h on the expression levels of FBXW7 in the 2D monolayers of MG-63 cells (Figure

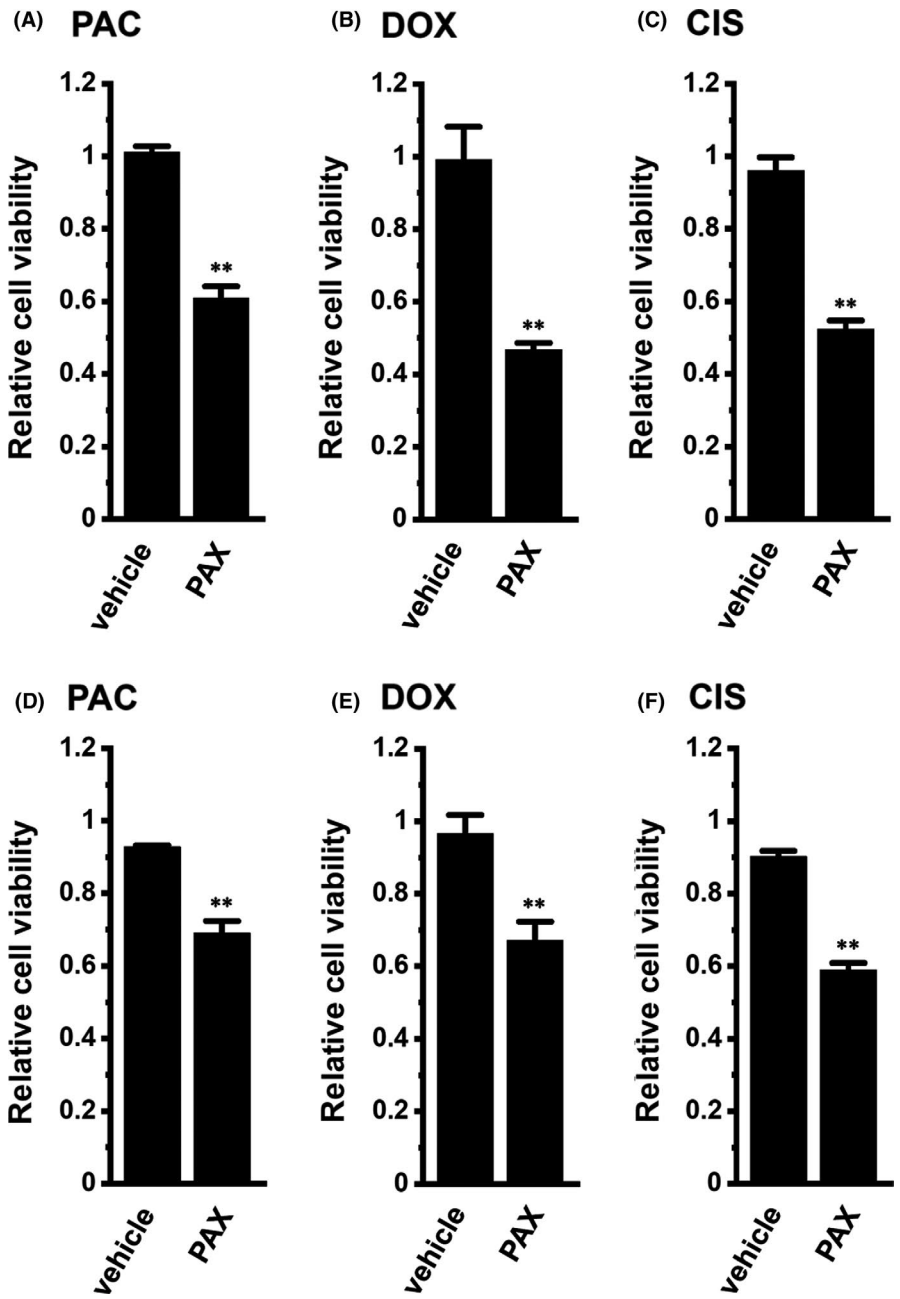

FIGURE 6 Effects of the treatment with the $K_{Ca}1.1$ inhibitor, PAX on chemoresistance acquired in MG-63 and SW-1353 spheroids. Effects of the treatment with 100 nmol/L PAC, 1 μmol/L DOX, and 10 μmol/L CIS for 48 h on cell viability in vehicle- and PAX-treated MG-63 (A-C) and SW-1353 (D-F) spheroids. The viability in the untreated cells with PAX was expressed as 1.0. Results are expressed as means ± SEM. $^{**}P < .01$ vs vehicle control

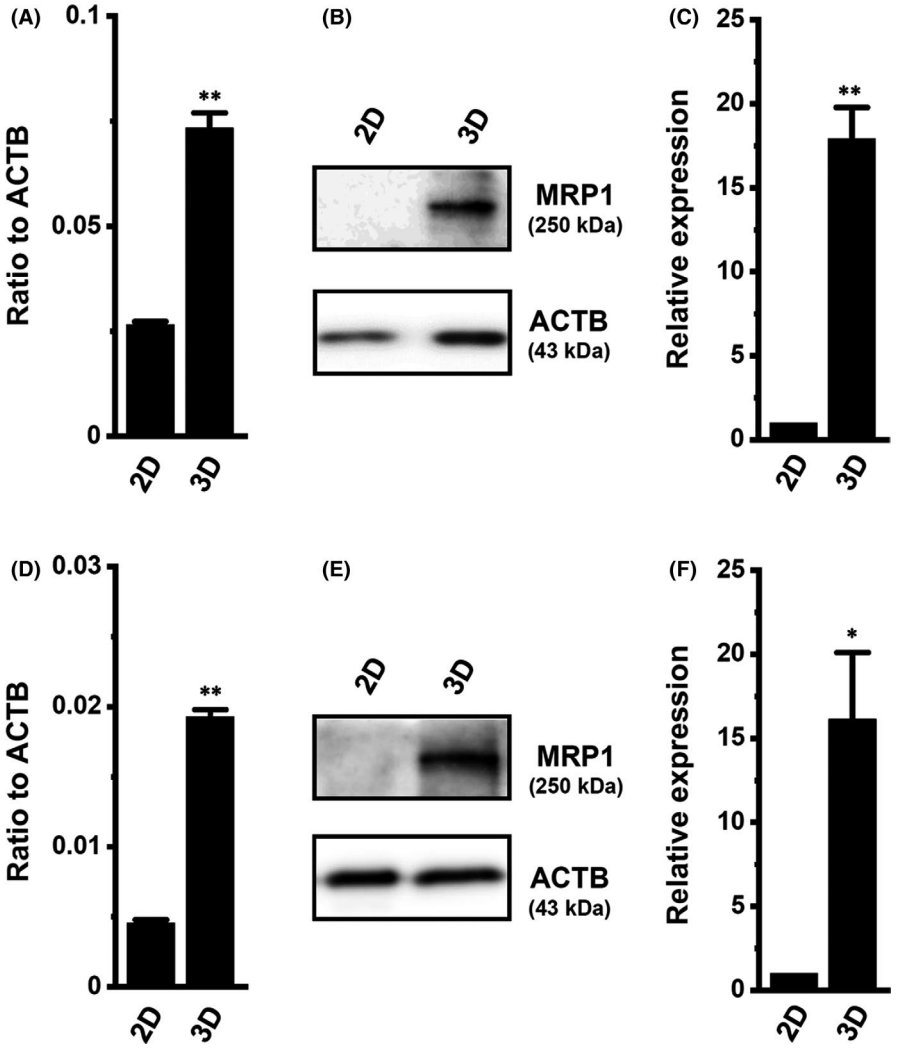

FIGURE 7 Increased expression of MRP1 in sarcoma spheroids. Real-time PCR examination of MRP1 transcripts in the 2D monolayers ("2D") and 3D spheroids ("3D") of MG-63 (A) and SW-1353 (D; n = 4 for each). Expression levels are shown as a ratio compared with ACTB. Protein expression of MRP1 in the lipid raft-enriched protein lysates of both groups. Blots were probed with anti-MRP1 (approximately 250 kDa) and anti-ACTB (43 kDa) antibodies (B, E). Summarized results were obtained as the optical density of MRP1 (C, F) band signals. After compensation for the optical density of the MRP1 protein band signal with that of the ACTB signal, optical density in "2D" was expressed as 1.0 (n = 4 for each). Results are expressed as means ± SEM. *, **$P < .05, .01$ vs 2D

S4). In 2D monolayers, the expression levels of FBXW7 were significantly decreased by NCO-01, but not vorinostat (Figure 10A). These results suggested that FBXW7-mediated $K_{Ca}1.1$ protein degradation was regulated by SIRT1 in MG-63 cells. We then examined the effects of HDAC inhibitor treatments on $K_{Ca}1.1$ protein expression in MG-63 cells. Consistent with these results, the expression levels of the $K_{Ca}1.1$ protein were increased by NCO-01, but not vorinostat in 2D-cultured MG-63 cells (n = 4 for each, $P < .05$; Figure 10B,C). No significant changes in the expression level of the $K_{Ca}1.1$ transcript by the SIRT1 inhibition were observed in 2D-cultured MG-63 cells (Figure 10D). There results suggested that FBXW7 is a downstream target of SIRT1 and that the SIRT1-FBXW7-$K_{Ca}1.1$ axis plays a pivotal role in poor prognosis and chemoresistance in $K_{Ca}1.1$-expressing solid cancers.

3.5 | Potential involvement of NRF2 in $K_{Ca}1.1$ inhibition-induced MRP1 downregulation and overcoming chemoresistance in sarcoma spheroids

MRP1 was upregulated in sarcoma spheroids (Figure 7), and was mostly recovered by the $K_{Ca}1.1$ inhibition (Figure 8). However, the underlying mechanisms remain unclear. Activation of the transcription factor NRF2 contributed to the acquisition of chemoresistance through the upregulation of MRP1 in cancer spheres.[34,35] As shown in Figure 11, the expression levels of NRF2 transcripts were increased by spheroid formation in both sarcomas (n = 4 for each, $P < .01$ vs 2D; Figure 11A,G), and were reversed by $K_{Ca}1.1$ inhibition (10 μmol/L PAX) for 24 h (n = 4 for each, $P < .01$ vs PAX; Figure 11B,H). Treatment with the NRF2 inhibitor ML385 (10 μmol/L) for 48 h decreased MRP1 expression levels in both sarcoma spheroids (n = 4 for each, $P < .01$ vs vehicle control; Figure 11E,K). Heat shock factor 1 (HSF1), which controls chemoresistance in cancer,[36] was also increased by spheroid formation in both sarcomas (n = 4 for each, $P < .01$ vs 2D; Figure 11C,I), and this was reversed by $K_{Ca}1.1$ inhibition (10 μmol/L PAX; n = 4 for each, $P < .01$ vs PAX; Figure 11D,J). In contrast with NRF2, the treatment with the HSF1 inhibitor KRIBB11 (10 μmol/L) for 48 h did not affect MRP1 expression levels in either sarcoma spheroid (n = 4 for each, $P > .05$ vs vehicle control; Figure 11F,L). No significant changes were observed in the expression levels of the MRP1, NRF2, and HSF1 transcripts following PAX treatment in $K_{Ca}1.1$ negative-human prostate cancer PC-3 cells and human colorectal cancer HCT-116 cells (Figure S5). These results

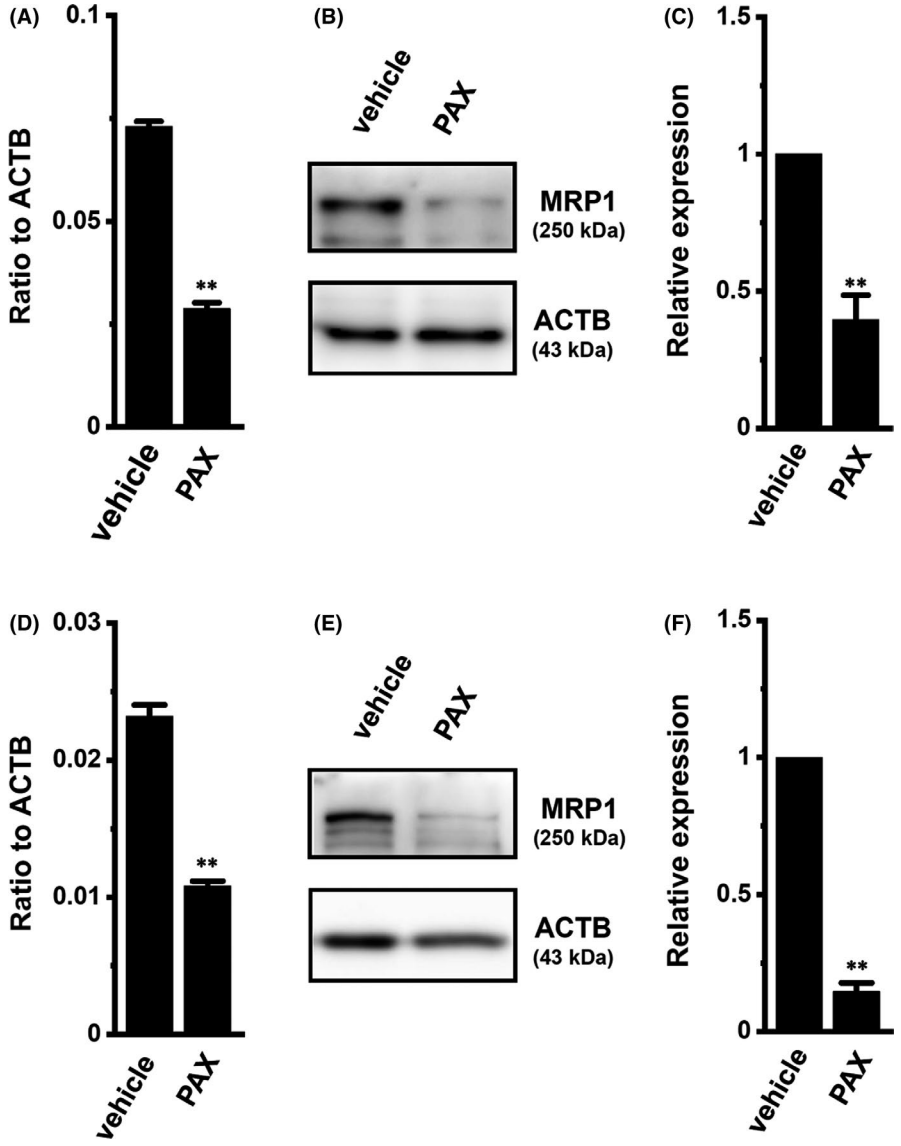

FIGURE 8 Decreased expression of MRP1 by the inhibition of $K_{Ca}1.1$ in sarcoma spheroids. Real-time PCR examination of MRP1 transcripts in vehicle- and PAX-treated MG-63 (A) and SW-1353 (D) spheroids (n = 4 for each). Expression levels are shown as a ratio compared with ACTB. Protein expression of MRP1 in the lipid raft-enriched protein lysates of both groups. Blots were probed with anti-MRP1 (approximately 250 kDa) and anti-ACTB (43 kDa) antibodies (B, E). Summarized results were obtained as the optical density of MRP1 (C, F) band signals. After compensation for the optical density of the MRP1 protein band signal with that of the ACTB signal, optical density in the vehicle control was expressed as 1.0 (n = 4 for each). Results are expressed as means ± SEM. $^{**}P < .01$ vs vehicle control

suggested that NRF2 is a critical transcriptional regulator of MRP1 in sarcoma spheroids, and appears to play a pivotal role in the overcoming of chemoresistance by the inhibition of $K_{Ca}1.1$.

4 | DISCUSSION

Cancer spheroid models constructed by 3D culture systems are widely utilized in cancer research. They exhibit physiologically relevant cell-cell and cell-matrix interactions, gene expression, and signaling pathway profiles that reflect in vivo tumors under hypoxic TME, and are applicable to in vitro chemosensitivity or chemoresistance assays.[37-39] Cancer spheroids exhibit growth arrest in the G_0 phase, similar to that in the quiescent region of TME. Riedl et al[40] reported that the number of cells in the S-phase was significantly lower in the 3D spheroids of various types of cancers than in 2D monolayers. In the present study, the cell cycle of MG-63 and SW-1353 spheroids was arrested at the G_1/S checkpoint (Figure S6). Additionally, we observed a positive correlation between hyperpolarization responses and $[Ca^{2+}]_i$ increases induced by the application of $K_{Ca}1.1$ activator in isolated cells from MG-63 and SW-1353 spheroids (Figure S7). The abundant expression of $K_{Ca}1.1$ in multiple cancer types has been attracting increasing interest in cancer research due to its crucial role in cancer-associated functions such as proliferation and metastasis. In the present study, human OS MG-63 cells and CS SW-1353 cells abundantly expressed $K_{Ca}1.1$ transcripts (Figures S1 and S2). However, the pathophysiological roles of $K_{Ca}1.1$ in cancer spheroids mimicking TME have not yet been elucidated. The main results of the present study are as follows:

(i) $K_{Ca}1.1$ activity was larger in MG-63 cells isolated from 3D spheroids than in those from 2D monolayers, together with a decrease in $K_{Ca}1.1$ protein degradation, but not transcriptional repression (Figure 1).

(ii) SIRT1-mediated FBXW7 downregulation caused a decrease in $K_{Ca}1.1$ protein degradation by spheroid formation in MG-63 cells (Figures 3, 4, 9, and 10).

(iii) $K_{Ca}1.1$ inhibition overcame acquired chemoresistance to PAC, DOX, and CIS by spheroid formation (Figures 5 and 6).

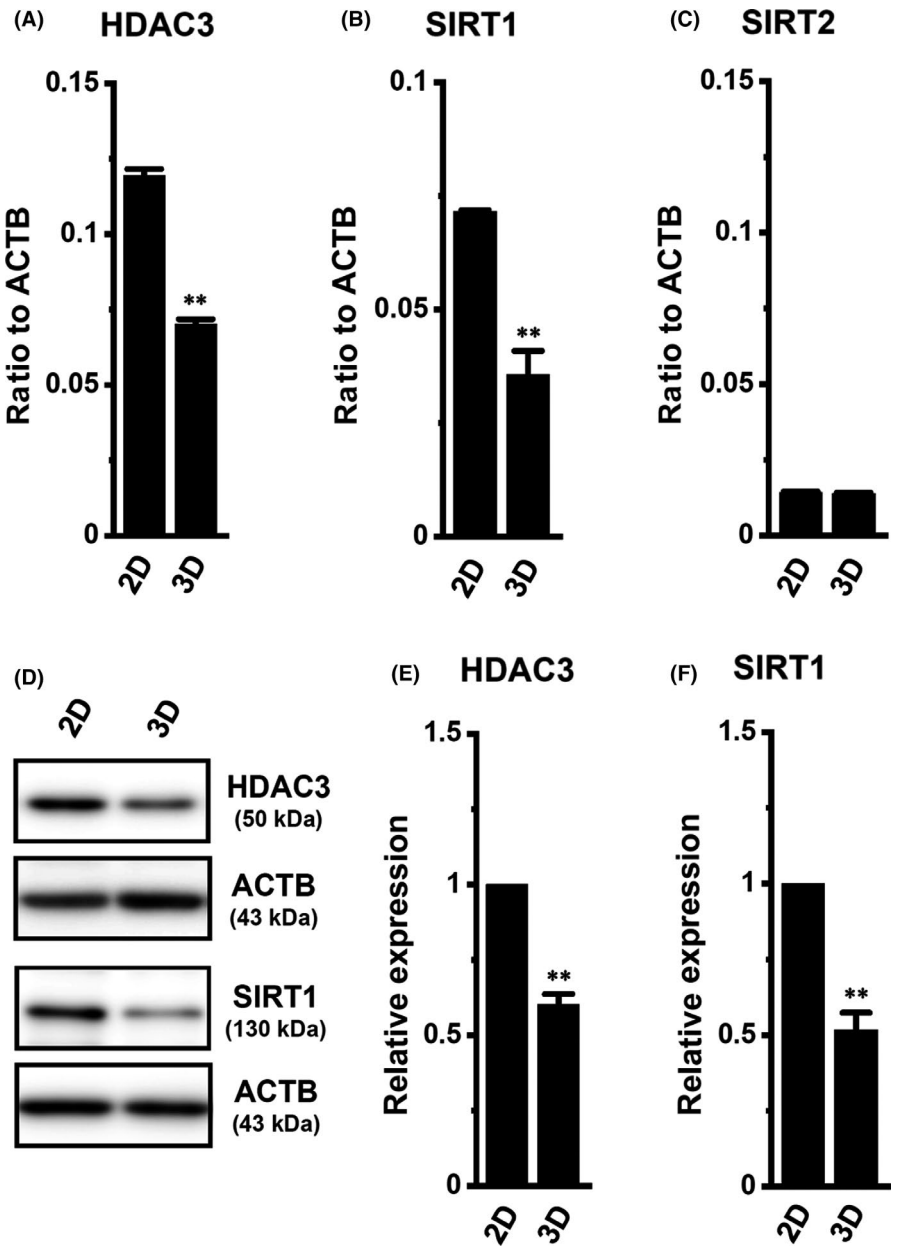

FIGURE 9 Decreased expression of HDAC3 and SIRT1 in MG-63 spheroids. Real-time PCR examination of HDAC3 (A), SIRT1(B), and SIRT2 (C) transcripts in 2D monolayers ("2D") and 3D spheroids ("3D") of MG-63 (n = 4 for each). Expression levels are shown as a ratio compared with ACTB. Protein expression of HDAC3 and SIRT1 in the protein lysates of both groups. Blots were probed with anti-HDAC3 (approximately 50 kDa), SIRT1 (approximately 130 kDa), and anti-ACTB (43 kDa) antibodies (D). Summarized results were obtained as the optical density of HDAC3 (E) and SIRT1 (F) band signals. After compensation for the optical density of the HDAC3 and SIRT1 protein band signals with that of the ACTB signal, optical density in "2D" was expressed as 1.0 (n = 4 for each). Results are expressed as means ± SEM. $^{**}P < .01$ vs 2D

(iv) Upregulation of MRP1 through NRF2 signaling pathways was associated with the acquisition of chemoresistance in both sarcoma spheroids, and $K_{Ca}1.1$ inhibition suppressed NRF2-mediated MRP1 expression (Figures 7, 8, and 11).

Collectively, the present results demonstrated that $K_{Ca}1.1$ is a key modulator of chemoresistance in sarcoma cells, indicating that targeting of $K_{Ca}1.1$ is a promising therapeutic strategy for overcoming chemoresistance.

The pluripotency-associated ubiquitin E3 ligase FBXW7 is a well known stemness regulator, and its downregulation is associated with an increase in stemness factors.[41] We previously demonstrated that FBXW7 was a key contributor to antiandrogen-induced $K_{Ca}1.1$ protein degradation in breast cancer cells.[27] As shown in Figure 1, the upregulated expression of the $K_{Ca}1.1$ protein in lipid raft fractions was observed in MG-63 spheroids, which increased $K_{Ca}1.1$ activity. Furthermore, FBXW7 was abundantly expressed in the 2D monolayers of MG-63 cells (Figure 3A-C), and the upregulated expression of the $K_{Ca}1.1$ protein was observed following siRNA-mediated FBXW7 inhibition (Figure 4). The expression level of FBXW7 was significantly lower in 2D monolayers of SW-1353 cells than in those of MG-63 cells (Figure 3D). Previous studies have reported that the ubiquitin E3 ligases MDM2 and CRBN also contributed to $K_{Ca}1.1$ protein degradation and regulated its activity.[27,30] As shown in Figure S3A,C, the expression level of MDM2 was increased in MG-63 and SW-1353 spheroids. The amplification of MDM2 is associated with poor prognosis in cancer patients, and its overexpression decreased survival rates and contributed to the acquisition of chemoresistance to DOX and CIS.[42] Similar to MDM2, the expression of CRBN was increased by spheroid formation in both cells (Figure S3B,D). These results strongly suggested that FBXW7 is a main contributor to $K_{Ca}1.1$ protein degradation in MG-63 spheroids, possibly in SW-1353 ones.

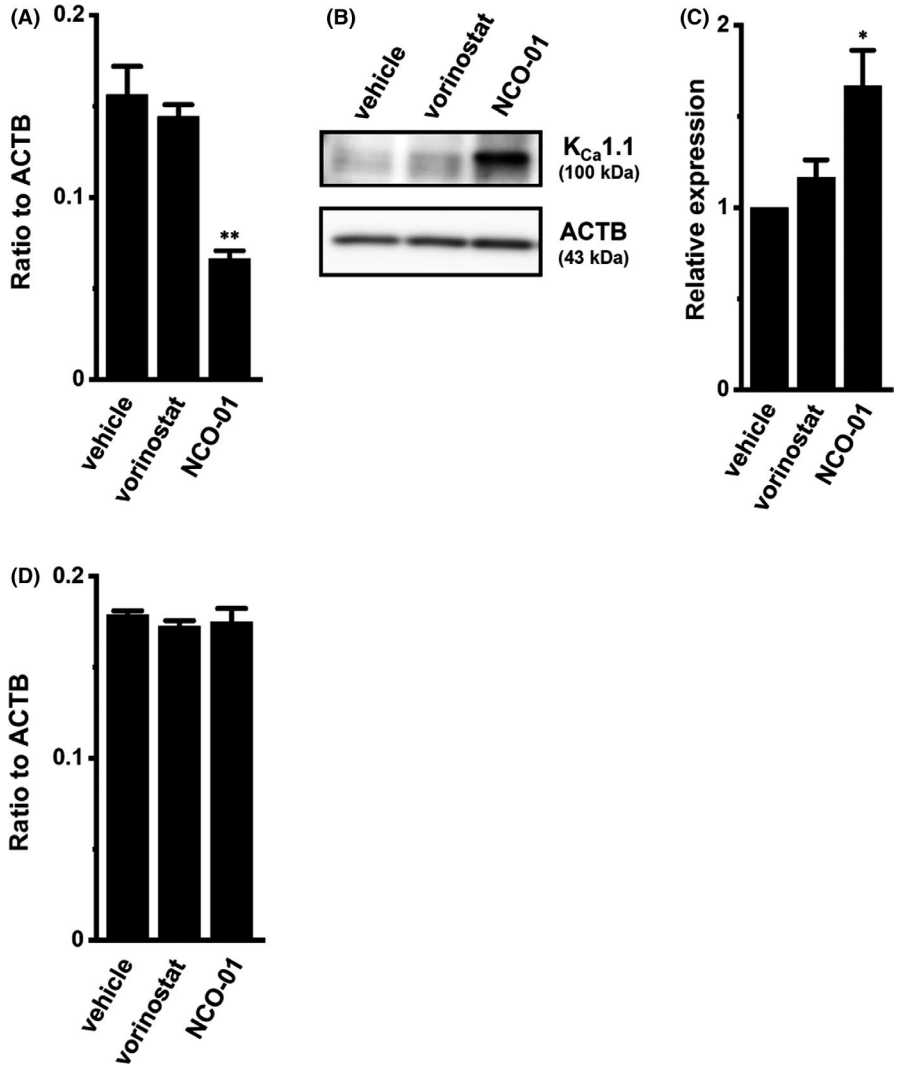

FIGURE 10 Decreased expression of FBXW7 and increased protein expression of K_{Ca}1.1 by SIRT1 inhibition in 2D-cultured MG-63 cells. Real-time PCR examination of FBXW7 (A) and K_{Ca}1.1 transcripts (D) in vehicle-, vorinostat (10 μmol/L)-, and NCO-01 (50 μmol/L)-treated, 2D-cultured MG-63 monolayers. Expression levels were shown as a ratio to ACTB. Protein expression of K_{Ca}1.1 in protein lysates of the vehicle-, vorinostat (10 μmol/L)-, and NCO-01 (50 μmol/L)-treated 2D monolayers of MG-63 cells. Blots were probed with anti-K_{Ca}1.1 (approximately 100 kDa) and anti-ACTB (43 kDa) antibodies (B). Summarized results were obtained as the optical density of K_{Ca}1.1 band signal (C). After compensation for the optical density of the K_{Ca}1.1 protein band signal with that of the ACTB signal, optical density in the vehicle control was expressed as 1.0 (n = 4 for each). Results are expressed as means ± SEM. $^{*}P < .05$, $^{**}P < .01$ vs vehicle control

The mechanisms underlying FBXW7 hypoexpression in MG-63 spheroids were examined. The class I and class III HDACs, HDAC3 and SIRT1 regulate hypoxia-induced metastasis and chemoresistance in a wide range of cancer types.[18,19] SIRT1 was previously shown to be downregulated in the hypoxic TME, resulting in poor prognosis and chemoresistance in some cancers.[20-22,43] As shown in Figure 9, decreased SIRT1 was detected in MG-63 spheroids. The decrease observed in FBXW7 expression was elicited by treatment with the SIRT1/2 inhibitor NCO-01 (50 μmol/L), but not the pan-HDAC inhibitor vorinostat (10 μmol/L) in the 2D monolayers of MG-63 cells (Figure 10A). SIRT1 inhibition increased K_{Ca}1.1 protein levels without changes to its gene transcription (Figure 10B-D). This work provides the first evidence to show the SIRT1-mediated modification of *FBXW7* gene expression. SIRT1 is known to be ubiquitinated by MDM2 E3 ligase.[44] Upregulated MDM2 (Figure S3) may contribute to decreases in SIRT1 in MG-63 spheroids. Alternatively, the activation of ERK1/2 decreased the expression of FBXW7 in cancer cells.[45] However, the ERK1/2 inhibitor SCH772984 (1 μmol/L) did not affect the transcription of *FBXW7* (Figure S8).

In the present study, K_{Ca}1.1 gene expression was not altered by HDAC modifications in MG-63 cells (Figure 10F). We have previously demonstrated that K_{Ca}1.1 transcription was upregulated by the pharmacological inhibition of the PI3K/AKT/mTOR signaling pathway.[27] Riedl et al[46] reported that the activation of the AKT/mTOR signaling pathway was reduced in cancer 3D spheroids. As shown in Figures 1G, 2F, no changes were observed in the expression levels of K_{Ca}1.1 transcripts between 2D monolayers and 3D spheroids in MG-63 and SW-1353 cells. However, the pharmacological inhibition of the PI3K/AKT/mTOR signaling pathway by LY294002 (10 μmol/L), AZD5363 (1 μmol/L), and everolimus (0.1 μmol/L) upregulated K_{Ca}1.1 transcription in both spheroids (Figure S9). These results may be due to the constitutive activation of the PI3K/AKT/mTOR signaling pathway in sarcoma.

Chemoresistance in cancer cells is mediated by numerous mechanisms including changes in the drug transporters that efflux anticancer drugs. The 3D culture was less sensitive to anticancer drugs than the 2D culture. The application of chemotherapeutic agents in clinical settings is limited, particularly due to the development of resistance. Our goal was to elucidate the molecular mechanisms underlying the development of chemoresistance. Chemoresistance is acquired by the upregulation of MRP1 in the TME of OS,[47] indicating that MRP1 is a key contributor to chemoresistance. The mechanism

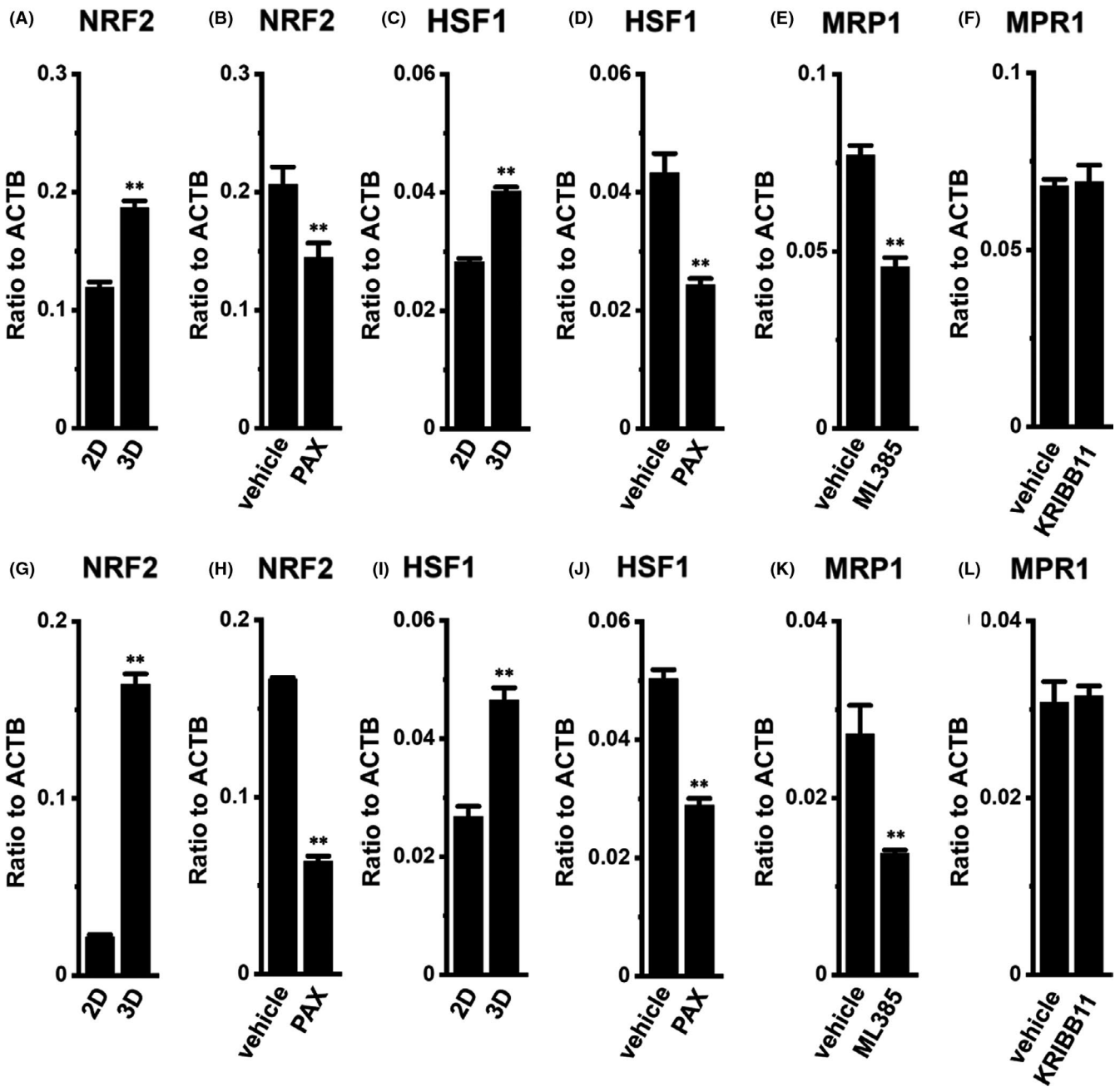

FIGURE 11 Increased expression of NRF2 transcripts decreases by inhibition with $K_{Ca}1.1$, and effects of NRF2 and HSF1 inhibitors on the expression of MRP1 transcripts in sarcoma spheroids. Real-time PCR examination of NRF2 and HSF1 in 2D- and 3D-cultured MG-63 (A, C) and SW-1353 cells (G, I) and in vehicle- and PAX (10 μmol/L)-treated (24 h) MG-63 (B, D) and SW-1353 spheroids (H, J). Real-time PCR examination of MRP1 in vehicle- and ML385 (10 μmol/L)-treated (for 24 h) MG-63 (E), and SW-1353 (K) spheroids and in vehicle- and KRIBB11 (10 μmol/L)-treated (for 24 h) MG-63 (F) and SW-1353 spheroids (L). Expression levels are shown as a ratio compared with ACTB. Results are expressed as means ± SEM. $^{**}P < .01$ vs "2D" or the vehicle control

of MRP1 functions is mainly a reduction in intracellular drug accumulation in the plasma membrane. The high expression of $K_{Ca}1.1$ was associated with the upregulation of MRP1, resulting in the acquisition of chemoresistance (Figure 5). Furthermore, pharmacological blockade of $K_{Ca}1.1$ decreased the expression of MRP1 in both sarcoma spheroids (Figure 6). Therefore, the inhibition of $K_{Ca}1.1$ is a promising therapeutic strategy for reversing chemoresistance in solid cancers. MRP1 is upregulated through the Notch1-NRF2 signaling pathways.[25,47-51] Li et al[47] showed that Notch1 was associated with MRP1 in OS.[51] In the present study, NRF2 was upregulated in both sarcoma spheroids (Figure 11A,G) and was suppressed by treatment with the $K_{Ca}1.1$ inhibitor (Figure 11B,H). In addition, the NRF2 inhibitor suppressed MRP1 expression in the 3D spheroids of both cells (Figure 11E,K). We examined the expression levels of Notch1 in 2D and 3D spheroids. However, its expression levels were low (less than 0.01 in arbitrary units) and no significant changes

were found. Mun et al[45] showed that HSF1 contributes to chemoresistance. HSF1 was also upregulated in both sarcoma spheroids (Figure 11C,I) and was suppressed by pretreatment with the $K_{Ca}1.1$ inhibitor (Figure 11D,J). However, no significant changes were observed in MRP1 expression by treatment with the HSF1 inhibitor in both sarcoma spheroids (Figure 11F,L). Therefore, $K_{Ca}1.1$ appears be an important regulator of NRF2-mediated MRP1 expression in $K_{Ca}1.1$-expressing sarcoma cells in vivo.

FBXW7 plays a prominent role in the induction of chemoresistance in cancer cells because its downregulated expression in several cancers resulted in the acquisition of chemoresistance,[52,53] however the underlying mechanisms have not yet been elucidated. The present results suggested that FBXW7 hypoexpression-induced enhancements in $K_{Ca}1.1$ activity may, at least partially, contribute to FBXW7-mediated chemoresistance.

In conclusion, the present results suggested that $K_{Ca}1.1$ serves as a critical chemoresistance-related molecule in human OS and CS cells. Chemoresistance is a significant factor associated with poor outcomes in sarcoma patients. Increased $K_{Ca}1.1$ levels upregulated MRP1, which reduced intracellular drug accumulation in the plasma membrane, in sarcoma spheroids. The inhibition of $K_{Ca}1.1$ may be a promising therapeutic strategy for reversing chemoresistance in human OS and CS. Mitochondrial ion channels are emerging as new oncological targets. A recent study focused on the crucial involvement of mitochondrial K^+ channels in chemoresistance in cancer cells.[54,55] Further studies are needed to elucidate the contribution of mitochondrial $K_{Ca}1.1$ to the mechanisms underlying chemosensitivity or chemoresistance in solid cancer.

ACKNOWLEDGMENTS

Medical English Service (Kyoto, Japan) reviewed the manuscript prior to its submission. This work was supported by the following source: A JSPS KAKENHI Grant [JP20K07071] (SO).

DISCLOSURE

The authors declare no conflicts of interest.

AUTHOR CONTRIBUTIONS

SO designed the study and wrote the initial draft of the manuscript. SO, JK, KE, MM, and HK contributed to data collection, analyses, and interpretation. EE and TS synthesized and quantitatively estimated HDAC/SIRT inhibitors. All authors critically reviewed the manuscript, approved its final version, and agreed to be accountable for all aspects of the work in ensuring that questions related to the accuracy or integrity of any part of the work were appropriately investigated and resolved.

ORCID


Susumu Ohya https://orcid.org/0000-0002-5765-0667

REFERENCES

1. Prevarskaya N, Skryma R, Shuba Y. Ion channels in cancer: are cancer hallmarks oncochannelopathies. *Physiol Rev*. 2018;98(2):559-621.
2. Girault A, Ahidouch A, Ouadid-Ahidouch H. Roles for Ca^{2+} and K^+ channels in cancer cells exposed to the hypoxic tumour microenvironment. *Biochim Biophys Acta Mol Cell Res*. 2020;1867(4):118644.
3. Oeggerli M, Tian Y, Ruiz C, et al. Role of KCNMA1 in breast cancer. *PLoS One*. 2012;7(8):e41664.
4. Ohya S, Kimura K, Niwa S, et al. Malignancy grade-dependent expression of K^+-channel subtypes in human prostate cancer. *J Pharmacol Sci*. 2009;109(1):148-151.
5. Latorre R, Castillo K, Carrasquel-Ursulaez W, et al. Molecular determinants of BK channel functional diversity and functioning. *Physiol Rev*. 2017;97(1):39-87.
6. Gonzalez-Perez V, Lingle CJ. Regulation of BK channels by beta and gamma subunits. *Annu Rev Physiol*. 2019;81:113-137.
7. Guéguinou M, Gambade A, Félix R, et al. Lipid rafts, KCa/ClCa/Ca2+ channel complexes and EGFR signaling: novel targets to reduce tumor development by lipids? *Biochim Biophys Acts*. 2015;1848(10 Pt B):2603-2620.
8. Jackson TM, Bittman M, Granowetter L. Pediatric malignant bone tumors: a review and update on current challenges, and emerging drug targets. *Curr Probl Pediatr Adolesc Health Care*. 2016;46(7):213-228.
9. Martin E, Senders JT, Ter Wengel PV, Smith TR, Broekman MLD. Treatment and survival of osteosarcoma and Ewing sarcoma of the skull: a SEER database analysis. *Acta Nerochir*. 2019;161(2):317-325.
10. Leddy LR, Holmes RE. Chondrosarcoma of bone. *Cancer Treat Res*. 2014;162:117-130.
11. Henney NC, Li BO, Elford C, et al. A large-conductance (BK) potassium channel subtype affects both growth and mineralization of human osteoblasts. *Am J Physiol Cell Physiol*. 2009;297(6):C1397-C1408.
12. Suzuki Y, Ohya S, Yamamura H, Giles WR, Imaizumi Y. A new splice variant of large conductance Ca^{2+}-activated K^+ (BK) channel α subunit alters human chondrocyte function. *J Biol Chem*. 2016;291(46):24247-24260.
13. Petrova V, Annicchiarico-Petruzzelli M, Melino G, Amelio I. The hypoxic tumour microenvironment. *Oncogenesis*. 2018;7(1):10.
14. Yuan Y, Jiang YC, Sun CK, Chen QM. Role of the tumor microenvironment in tumor progression and the clinical applications (Review). *Oncol Rep*. 2016;35(5):2499-2515.
15. Xia Y, Jiang L, Zhong T. The role of HIF-1α in chemo-/radioresistance tumors. *Onco Targets Ther*. 2018;11:3003-3011.
16. Calpe B, Kovacs WJ. High-throughput screening in multicellular spheroids for target discovery in the tumor microenvironment. *Expert Opin Drug Discov*. 2020;15(8):955-967.
17. Nunes AS, Barros AS, Costa EC, Moreira AF, Correia IJ. 3D tumor spheroids as in vitro models to mimic in vivo human solid tumors resistance to therapeutic drugs. *Biotechnol Bioeng*. 2019;116(1):206-226.
18. Gao Y, Liu B, Feng L, et al. Targeting JUN, CEBPB, and HDAC3: a novel strategy to overcome drug resistance in hypoxic glioblastoma. *Front Oncol*. 2019;9:33.
19. Mvunta DH, Miyamoto T, Asaka R, et al. SIRT1 regulates the chemoresistance and invasiveness of ovarial carcinoma cells. *Transl Oncol*. 2017;10(4):621-631.
20. Lim JH, Lee YM, Chun YS, Chen J, Kim JE, Park JW. Sirtuin 1 modulates cellular responses to hypoxia by deacetylating hypoxia-inducible factor 1α. *Mol Cell*. 2010;38(6):864-878.
21. Shi L, Tang X, Qian M, et al. A SIRT1-centered circuitry regulates breast cancer stemness and metastasis. *Oncogene*. 2018;37(49):6299-6315.
22. Dong G, Wang B, An Y, et al. SIRT1 suppresses the migration and invasion of gastric cancer by regulating ARHGAP5 expression. *Cell Death Dis*. 2018;9(10):977.
23. Kischel P, Girault A, Rodat-Despoix L, et al. Ion channels: new actors playing in chemotherapeutic resistance. *Cancers*. 2019;11(3):376.

24. Loignon M, Miao W, Hu L, et al. Cul3 overexpression depletes Nrf2 in breast cancer and is associated with sensitivity to carcinogens, to oxidative stress, and to chemotherapy. *Mol Cancer Ther*. 2009;8(8):2432-2440.
25. Zhou Y, Xu X, Wu J, et al. Allyl isothiocyanate treatment alleviates chronic obstructive pulmonary disease through the Nef2-notch1 signaling and upregulation of MRP1. *Life Sci*. 2020;243:117291.
26. Hayashi A, Suzuki H, Itoh K, Yamamoto M, Sugiyama Y. Transcription factor Nrf2 is required for the constitutive and inducible expression of multidrug resistance-associated protein 1 in mouse embryo fibroblasts. *Biochem Biophys Res Commun*. 2003;310(3):824-829.
27. Khatun A, Shimozawa M, Kito H, et al. Transcriptional repression and protein degradation of the Ca^{2+}-activated K^+ channel $K_{Ca}1.1$ by androgen receptor inhibition in human breast cancer cells. *Front Physiol*. 2018;9:312.
28. Yumimoto K, Yamauchi Y, Nakayama KI. F-box proteins and cancer. *Cancers*. 2020;12(5):1249.
29. Gong J, Zhou Y, Liu D, Huo J. F-box proteins involved in cancer-associated drug resistance (Review). *Oncol Lett*. 2018;15(6):8891-8900.
30. Choi T-Y, Lee S-H, Kim Y-J, et al. Cereblon maintains synaptic and cognitive function by regulating BK channel. *J Neurosci*. 2018;38(14):3571-3583.
31. Rovey RW, Pluchino KM, Hall MD, Fojo AT, Bates SE, Gottesman MM. Revisiting the role of ABC transporters in multidrug-resistant cancer. *Nat Rev Cancer*. 2018;18(7):452-464.
32. Yeh CH, Bellon M, Nicot C. FBXW7: a critical tumor suppressor of human cancers. *Mol Cancer*. 2018;17(1):115.
33. Sailo BL, Banik K, Girisa S, et al. FBXW7 in cancer: what has been unraveled thus far? *Cancers*. 2019;11(2):246.
34. Ryoo IG, Kim G, Choi BH, Lee SH, Kwak MK. Involvement of NRF2 signaling in doxorubicin resistance of cancer stem cell-enriched colonospheres. *Biomol Ther*. 2016;24(5):482-488.
35. Bai X, Chen Y, Hou X, Huang M, Jin J. Emerging role of NRF2 in chemoresistance by regulating drug-metabolizing enzymes and efflux transporters. *Drug Metab Rev*. 2016;48(4):541-567.
36. Vydra N, Toma A, Glowala-Kosinska M, Gogler-Piglowska A, Widlak W. Overexpression of heat shock transcription factor 1 enhances the resistance of melanoma cells to doxorubicin and paclitaxel. *BMC Cancer*. 2013;13:504.
37. Nath S, Devi GR. Three-dimensional culture system in cancer research: Focus on tumor spheroid model. *Pharmacol Ther*. 2016;163:94-108.
38. Ishiguro T, Ohata H, Sato A, Yamawaki K, Enomoto T, Okamoto K. Tumor-derived spheroids: relevance to cancer stem cells and clinical applications. *Cancer Sci*. 2017;108(3):283-289.
39. Sant S, Johnston PA. The production of 3D tumor spheroids for cancer drug discovery. *Drug Discov Today Technol*. 2017;23:27-36.
40. Riedl A, Schlederer M, Pudelko K, et al. Comparison of cancer cells in 2D vs 3D culture reveals differences in AKT-mTOR-S6K signaling and drug responses. *J Cell Sci*. 2017;130(1):203-218.
41. Okita Y, Matsumoto A, Yumimoto K, Isoshita R, Nakayama KI. Increased efficiency in the generation of induced pluripotent stem cells by Fbxw7 ablation. *Genes Cells*. 2012;17(9):768-777.
42. Tracz-Gaszewska Z, Klimczak M, Biecek P, et al. Molecular chaperones in the acquisition of cancer cell chemoresistance with mutated *TP53* and MDM2 up-regulation. *Oncotarget*. 2017;8(47):82123-82143.
43. An Y, Wang B, Wang X, Dong G, Jia J, Yang Q. SIRT1 inhibits chemoresistance and cancer stemness of gastric cancer by initiating an AMPK/FOXO3 positive feedback loop. *Cell Death Dis*. 2020;11(2):115.
44. Peng L, Yuan Z, Li Y, et al. Ubiquitinated sirtuin 1 (SIRT1) function is modulated during DNA damage-induced cell death and survival. *J Biol Chem*. 2015;290(14):8904-8912.
45. Mun GI, Choi E, Lee Y, Lee YS. Decreased expression of FBXW7 by ERK1/2 activation in drug-resistant cancer cells confers transcriptional activation of MDR1 by suppression of ubiquitin degradation of HSF1. *Cell Death Dis*. 2020;11(5):395.
46. Riedl A, Schlederer M, Pudelko K, et al. Comparison of cancer cells in 2D vs 3D culture reveals differences in AKT-mTOR-S6K signaling and drug responses. *J Cell Sci*. 2017;130(1):203-218.
47. Li C, Guo D, Tang B, Zhang Y, Zhang K, Nie L. Notch1 is associated with the multidrug resistance of hypoxic osteosarcoma by regulating MRP1 gene expression. *Neoplasma*. 2016;63(5):734-742.
48. Udasin RG, Wen X, Bircsak KM, et al. Nrf2 regulates the sensitivity of mouse keratinocytes to nitrogen mustard via multidrug resistance-associated protein 1 (Mrp1). *Toxicol Sci*. 2016;149(1):202-212.
49. Kim B, Stephen SL, Hanby AM, et al. Chemotherapy induces Notch1-dependent MRP1 up-regulation, inhibition of which sensitizes breast cancer cells to chemotherapy. *BMC Cancer*. 2015;15:634.
50. Zhang Z, Zhou Z, Zhang M, et al. High Notch1 expression affects chemosensitivity of head and neck squamous cell carcinoma to paclitaxel and cisplatin treatment. *Biomed Pharmacother*. 2019;118:109306.
51. Wakabayashi N, Chartoumpekis DV, Kensler TW. Crosstalk between Nrf2 and Notch signaling. *Free Radic Biol Med*. 2015;88(Pt B):158-167.
52. Xiao G, Li Y, Wang M, et al. FBXW7 suppresses epithelial-mesenchymal transition and chemo-resistance of non-small-cell lung cancer cells by targeting snai1 for ubiquitin-dependent degradation. *Cell Prolif*. 2018;51(5):e12473.
53. Lorenzi F, Babaei-Jadidi R, Sheard J, Spencer-Dene B, Nateri AS. Fbxw7-associated drug resistance is reversed by induction of terminal differentiation in murine intestinal organoid culture. *Mol Ther methods Clin Dev*. 2016;3:16024.
54. Bachmann M, Costa R, Peruzzo R, Prosdonimi E, Checchetto V, Leanza L. Targeting mitochondrial ion channels to fight cancer. *Int J Mol Sci*. 2018;19(7):2060.
55. Peruzzo R, Szabo I. Contribution of mitochondrial ion channels to chemo-resistance in cancer cells. *Cancers*. 2019;11(6):761.

SUPPORTING INFORMATION

Additional supporting information may be found online in the Supporting Information section.

How to cite this article: Ohya S, Kajikuri J, Endo K, Kito H, Elboray EE, Suzuki T. Ca^{2+}-activated K^+ channel $K_{Ca}1.1$ as a therapeutic target to overcome chemoresistance in three-dimensional sarcoma spheroid models. *Cancer Sci*. 2021;112:3769–3783. https://doi.org/10.1111/cas.15046